Available online at www.sciencedirect.com
SCIENCE DIRECT®
ELSEVIER
Journal of Solid State Chemistry 177 (2004) 1480–1487
JOURNAL OF SOLID STATE CHEMISTRY
http://elsevier.com/locate/jssc

Preparation and characterization of Al and Mn doped ZnO (ZnO: (Al, Mn)) transparent conducting oxide films

H.T. Cao,* Z.L. Pei, J. Gong, C. Sun, R.F. Huang, and L.S. Wen

Department of Surface Engineering of Materials, Institute of Metal Research, The Chinese Academy of Sciences, Shenyang 110016, PR China

Received 20 July 2003; received in revised form 23 October 2003; accepted 25 November 2003

Abstract

This paper presents the electro-optical, chemical and structural properties of doped-ZnO films deposited by DC-reactive magnetron sputtering at room temperature using the bi-dopant Al and Mn. A minimum resistivity of $3.46 \times 10^{-4}\,\Omega\,\mathrm{cm}$, exceeding 75.0% average transmittance (380–800 nm), and fundamental band gap of 3.48 ± 0.01 eV have been obtained. XPS analyses show that Zn uniformly remains in the valence state of Zn^{2+}; all of the Al and a little amount of Mn with valence state of Mn^{4+} are supposed to have donor effect, while dominant Mn^{2+} will induce to form more oxygen vacancies and this proposal has been verified by O 1*s* XPS results. It has been concluded that the presence of more oxygen vacancies will attenuate the effect of hybridization of $p-d$ orbitals in the matrix of ZnO. It has been found that all the as-deposited films have *c*-axis preferred orientation with flat and smooth surface (RMS surface roughness is of the order of ~ 3 nm over $5 \times 5\,\mu\mathrm{m}^2$ area).
© 2003 Elsevier Inc. All rights reserved.

PACS: 81.15.Cd; 73.61.Ga; 78.66.Hf; 82.80.Pv; 68.55.Jk

Keywords: DC reactive magnetron sputtering; Transparent conducting oxide; Electro-optical properties; XPS; Structural properties

1. Introduction

ZnO has a filled O^{2-}: 2*p* valence band, and the O^{2-}: 2*p* states are bonding while the Zn: 4*s* states are anti-bonding. It features a wide band gap (3.437 eV at 2 K [1]) non-stoichiometric n-type semiconductor with a low resistivity ($\sim 10^{-3}\,\Omega\,\mathrm{cm}$) and high transmittance ($\approx 90\%$) in the visible solar region. The resistivity can be reduced further to the range of $10^{-4}\,\Omega\,\mathrm{cm}$ by doping without sacrificing luminous transparency. The unique nature makes it suitable for wide applications such as energy efficiency windows, smart windows, and electrodes for solar cells as well as flat-panel displays, etc. [2]. In comparison with other host oxides like CdO, In_2O_3 and SnO_2, ZnO has attracted intensive interest because of its non-toxicity, low cost, excellent adhesion to the substrate, easily etching ability besides common electro-optical properties. Furthermore, zinc oxide is more chemically stable than tin or indium oxide films when exposed to hydrogen plasma [3]. B, Al, Ga, In (Group III A), Si, Ge (Group IV A), Ti, Zr, Hf (Group IV B) and Sc, Y (Rare earth element) are the most used doping agents for ZnO [4–10]. However, both the chemical and physical properties of currently utilized transparent conducting oxides (TCOs) besides impurity-doped ZnO are far from optimum. Improvement in performance of TCOs is desirable because their non-ideal properties will eventually ruin the complete device performance. For this purpose, the TCO community must either find better ways of optimizing the conventional TCOs or explore more complex new materials with tailorable structural, physical and chemical properties. It is speculated that the latter case is more fruitful than the former because of voluminous literature devoted to optimization of TCO film deposition without satisfying results. This paper is performed to explore Al and Mn doped zinc oxide films and understand their properties.

2. Experimental

Sputtering of ZnO: (Al, Mn) films on quartz or corning 7059 glass substrate (parallel to the target

*Corresponding author. Fax: +86-24-2384-3436.
E-mail addresses: htcao@imr.ac.cn (H.T. Cao), csun@imr.ac.cn (C. Sun).

0022-4596/$ - see front matter © 2003 Elsevier Inc. All rights reserved.
doi:10.1016/j.jssc.2003.11.030

surface) was performed at room temperature using a conventional planar DC reactive magnetron sputtering system, a technique characteristic of the ease of controlling deposition parameters and growing high quality films without additional heating. A special advantage of low temperature deposition was found necessary to avoid a degradation of the interface by elements interdiffusion. Two different alloy targets were used in this work. The composition of the first was Zn-1.50Al-0.20Mn (wt%, tagged A#) and the composition of the second was Zn-0.75Al-1.50Mn (tagged B#). The target to substrate distance was fixed at 7 cm. Before deposition, the chamber was evacuated to an ultimate background pressure better than 3×10^{-3} Pa and then a pre-sputtering process was employed for 2 min to clean the target surface. The working gas Ar and O_2 were independently metered by two mass flow controllers. The argon was directly introduced to the surface of the target while oxygen was leaked into the chamber far away from target and substrate. Consequently, it was difficult to describe exactly the O_2 partial pressure in the chamber, thus the $O_2/(Ar+O_2)$ flux ratio (hereafter referred to as O_2 partial pressure P_{O_2}) was used as an indicator instead of the actual O_2 partial pressure. Working pressure was in the range from 0.5 to 0.7 Pa. Electrical properties of the films was measured at room temperature by a simple DC four-point probe system as well as a Hall measurement system with the Van de Pauw configuration. The transmittance and reflectance spectra were recorded with a HITACHI U-3400 spectrophotometer within the wavelength from 190 to 1500 nm. The samples were mounted into a LAS-3000 surface analysis system for X-ray photoelectron spectroscopy (XPS) analysis of the original surfaces, and then the films were sputtered at different intervals by an Argon ion gun operated at 2.5 keV (etching rate 1.5 nm min^{-1}) followed by XPS acquisition after each time step. The XPS spectra were recorded using monochromatic Mg*K*α excitation (1253.6 eV). All the XPS spectra were referenced to C1*s* peak (284.7 eV). Crystallographic and phase structure were determined by an X-ray diffractometer (Rigaku) with Cu*K*α radiation. The surface topography and film thickness (with step) were investigated using a Nanosope IIIa atomic force microscope (AFM).

3. Results and discussion

3.1. Electrical and optical properties

The electrical properties of TCOs films depend on external preparation parameters like doping level, discharge power, oxygen partial pressure, and the target to substrate distance etc., and the results are different for different workers. Fig. 1(a) shows the variations of resistivity of ZnO: (Al, Mn) films with target type as a function of oxygen partial pressure. According to the criterion that films with lower resistivity as well as good transparency, it is observed that target B# has an advantage over A# in a wide range of oxygen partial pressure. From the Hall measurement it is revealed that the Hall mobility of the films deposited using target B# are always larger than those of the films from target A# while the differences of carrier concentration between them are marginal under the same deposition condition. Therefore, it is speculated that the entry of more Mn atoms as mineralizers or/and surfactants into the films is likely to result in higher quality of film crystallinity, which is responsible for enhancing the Hall mobility. Fig. 1(b) exhibits dependence of resistivity on deposition voltage. The higher the deposition voltage, the more the kinetic energy of sputtered particles. The additional energy inputting into the film causes an increased surface mobility of the adatoms that will in turn improve the film perfection, i.e. the enhanced migration of sputtered particles will cause desorption of oxygen adsorbed on the grain boundary. The variations of resistivity with oxygen partial pressure are depicted in Fig. 1(c). Resistivity (ρ) is very sensitive to P_{O_2}, both Hall mobility (μ) and carrier concentration (N) are very sensitive to it as well. A minimal resistivity of $3.46\times10^{-4}\,\Omega$ cm with a Hall mobility of 32.54 cm^{2}V^{-1}s^{-1} and a carrier density of 5.55×10^{20} cm^{-3} is obtained at $P_{O_2}=0.32$ (target B#, 320 V voltage, 1.6 W cm^{-2} discharge power, 230 nm thickness), which is comparable to formerly reported results [11,12]. When oxygen partial pressure ranges from 0.28 to 0.25, it is revealed that the resistivity increases with decrease in P_{O_2}. This increase in ρ is due to shallow donors or/and relative deep donors partially lose their dopant effect and consequently reduce the carrier concentration, meanwhile the Hall mobility is improved, thereby the presence of severe oxygen deficiencies that can deteriorate the crystalline properties and generate more free electrons in the conduction band can be ruled out. When P_{O_2} lower than 0.25 (not shown here), severe oxygen deficiencies may dominate, giving rise to metal-like darken films with higher resistivity to be formed. As P_{O_2} is in the region of 0.28–0.32, resistivity decreases with oxygen partial pressure increasing. The decrease can be ascribed to the improvement of crystallization that can enhance the mobility of the carriers while the carrier concentration fluctuating mildly. A further increasing P_{O_2} (not shown here either) will favor the films approach stoichiometry, resulting in no increase or even a decrease in conductivity. The electron mobility depends on several scattering mechanisms such as grain boundary and ionized impurity scattering, which is described elsewhere [13].

The window of transparency to electromagnetic radiation at low energy for ZnO is limited by the

Fig. 1. (a) Variations of resistivity with different targets as a function of oxygen partial pressure (voltage 320 V), some Hall mobility values are shown in the parentheses, (b) variations of resistivity with different deposition voltage as a function of oxygen partial pressure (B# target), (c) resistivity (ρ), carrier concentration (N) and Hall mobility (μ) for ZnO: (Al, Mn) films vs. oxygen partial pressure.

conduction electron plasma energy $\hbar\omega_p$; the high-energy limit to transparency is defined by the onset of absorption from valence band states of dominant O^{2-}: $2p$ into Zn: $4s$ conduction band states. The paramount factor affecting the optical properties is expected to be the carrier concentration rather than electron mobility. Fig. 2 contains integrated transmittance for representative ZnO: (Al, Mn) films. The average transmittance (without glass substrate deduction) in the visible region within the wavelength from 380 to 800 nm is more than 75.0% for all specimens. As depicted in Fig. 2, the higher the carrier density, the better transmittance at shorter wavelengths. It is mainly due to the wavelength of the absorption edge being shifted toward the higher energy side with increasing electron density. In the near-infrared (IR), however, the transmittance decrease with higher carrier concentration is owing to plasma resonance.

For ZnO with direct allowed transition band structure, the apparent band gap can be determined from the squared absorption coefficient vs. photon energy by using the following formula:

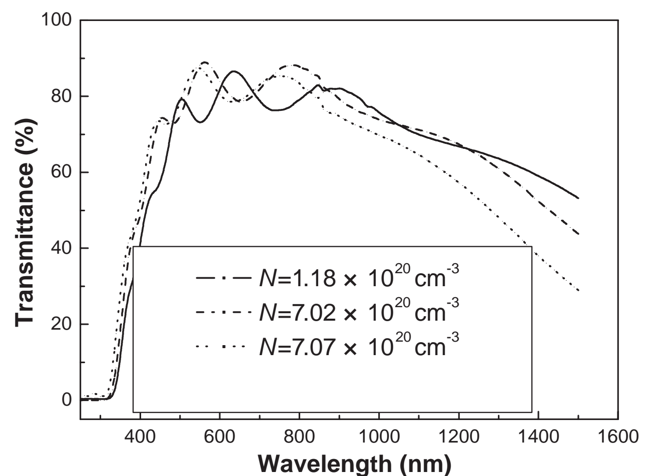

Fig. 2. Transmittance of ZnO: (Al, Mn) films with various carrier concentrations (as-deposited, film thickness 230 nm).

$$\alpha h\gamma \simeq (h\gamma - E_{\text{opt}})^{1/2}, \qquad (1)$$

where $h\gamma$ is the photon energy and E_{opt} is the apparent band gap. The optical absorption coefficient α is obtained from optical spectroscopy measurement. Assuming that both the conduction band and valence band are parabolic and the Fermi plane is spherical, the variation of band gap is based on Burstein-Moss effect [14] without regard to the many-body effect [15] that can shrink the band gap and compensate the band gap widening due to the conduction band occupancy blocks states at the bottom of the conduction band.

$$E_{opt} = E_{g0} + \frac{\hbar^2(3\pi^2)^{2/3}N^{2/3}}{2}\left(\frac{1}{m^*_{d(c)}} + \frac{1}{m^*_{d(v)}}\right), \quad (2)$$

$$\left(\frac{1}{m^*_{d(c)}} + \frac{1}{m^*_{d(v)}}\right) = \frac{1}{m^*_{cv}}, \quad (3)$$

where E_{g0} is fundamental band gap, $m^*_{d(c)}$, $m^*_{d(v)}$, m^*_{cv} is conduction band density-of-states effective mass, valence band density-of-states effective mass and reduced effective mass of electron, respectively. The band gap is found directly proportional to $N^{2/3}$, i.e. the width of the occupied Zn: 4*s* conduction band is broadened with higher carrier density. The E_{g0}, 3.48 ± 0.01 eV, and the fundamental absorption edge, 356.5 ± 1.0 nm, are also obtained for ZnO: (Al, Mn) films.

3.2. Chemical properties

A typical ZnO: (Al, Mn) specimen with a thickness of 230 nm was carried out for XPS analysis. The specimen was prepared under the optimal deposition conditions as follows: target B#, $P_{O_2} = 0.32$, 320 V voltage, 1.6 W cm^{-2} discharge power. Although the sample was rinsed using standard protocols before XPS experiment, its original surface was still contaminated with adventitious carbon (C 1*s* with 284.7 eV binding energy). After Argon ion bombardment, the feature of carbon can be removed from the surface. The spectra of Zn $2p_{3/2}$ with curve-fitting results are shown in Fig. 3. For Zn $2p_{3/2}$

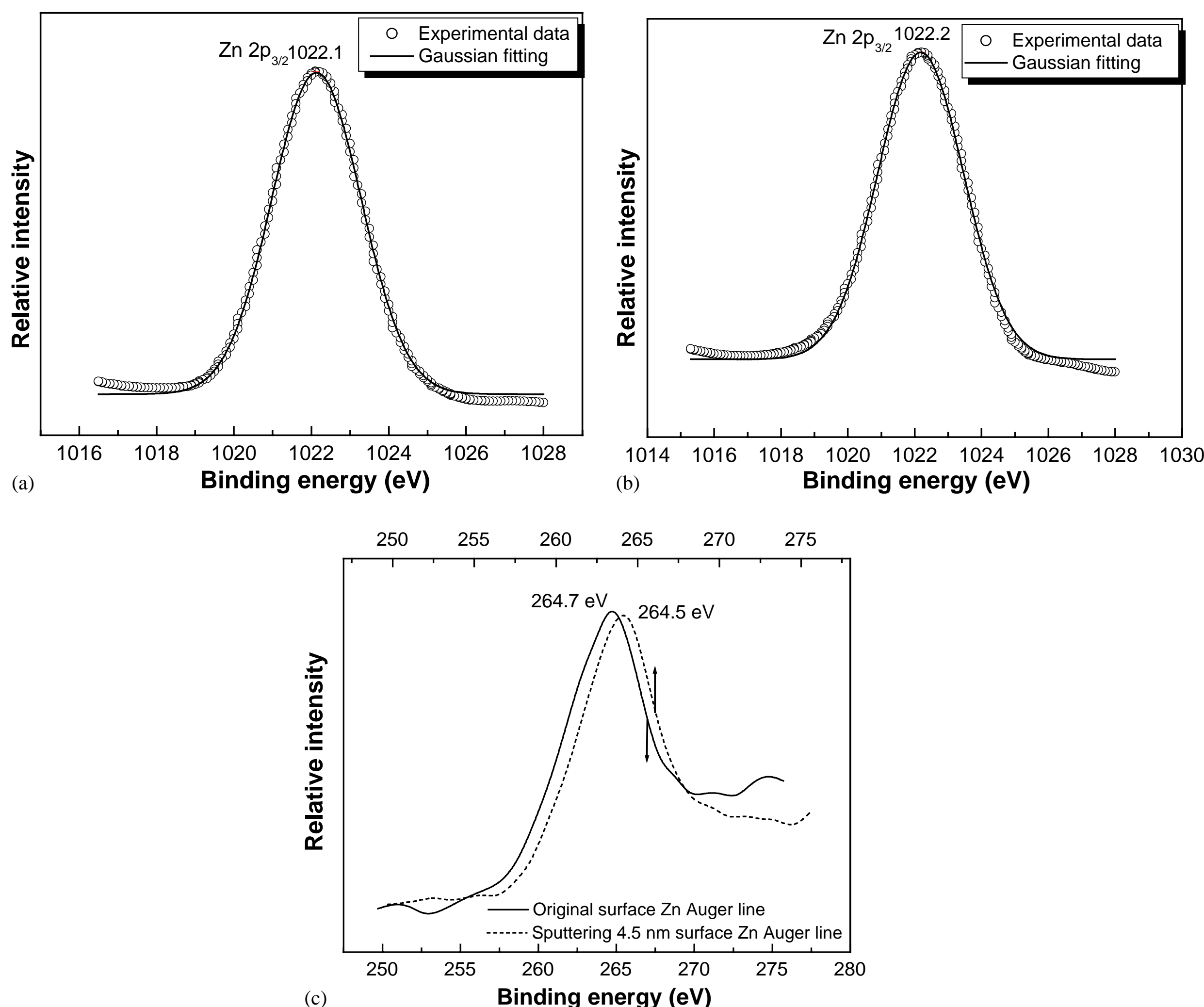

Fig. 3. XPS spectra in the Zn $2p_{3/2}$ region. (a) Original surface, (b) after Ar$^+$ etching 4.5 nm, and (c) the binding energy of Zn ($L_3M_{45}M_{45}$) Auger transition before and after Ar$^+$ bombardment 4.5 nm.

core level centered at 1022.1 eV, no changes concerning the spectra position and shape are observed in both original and new surface after Ar^+ etching 4.5 nm, indicating that there is no measurable change in the chemical state of Zn^{2+} [3]. Fig. 3(c) exhibits the binding energy of Zn ($L_3M_{45}M_{45}$) Auger transition (around 265 eV). We note that the corresponding binding energy of metallic Zn is 260.2 eV [3], which further confirms the uniform oxidation state of Zn^{2+}.

For some unknown reasons, the Al and Mn $2p_{3/2}$ core levels are not detectable in the as-received surface but occur after Ar^+ bombardment, as seen in Fig. 4. The slight variation of dopant content at depth profile inside the film was also observed by Hong et al. [16]. The Al $2p_{3/2}$ is broad and can be fitted with a single lorentzian function, showing distinct lorentzian character. From the Al $2p_{3/2}$ peak centered at 73.85 eV, it has been observed evidence of ESCA peak from Al^{3+} rather than metallic Al. It is considered that Al ions dissolved in ZnO matrix substitute Zn successfully and form weakly bonded electrons that contribute the conductivity. The broad and asymmetric of Mn $2p_{3/2}$ peak, implying the presence of a multi-component of Mn, can be disconvoluted by the best fitting with Gaussian function into three peaks. The left centered at 637.7 eV with the full width at half maximum (FWHM) of 1.99 eV can be assigned to metallic Mn; the intermediate peak centered at 640. 4 eV with HWHM of 2.09 eV is due to the chemical state of Mn^{2+}; the right centered at 642.4 eV with FWHM of 1.87 eV can be allocated to Mn^{4+}, as displayed in Fig. 4 (b). Where the metallic Mn indwells and the effect of them is not clear. Let us focus the chemical states of Mn^{4+} and Mn^{2+}. From the data of the standard Gibbs formation energy, it seems that thermodynamics favors formation of MnO_2 and MnO ($\Delta_f G_m^\Theta(MnO_2) = -466.1$, $\Delta_f G_m^\Theta(MnO) = -362.8\,kJ\,mol^{-1}$). As for Mn^{4+}, its ion radii (radii (Mn^{4+}) = 0.054 nm) is smaller than that of Zn^{2+} (radii (Zn^{2+}) = 0.075 nm) while its nuclear charge is larger than that of Zn^{2+}, as a result, it can be assumed that the Mn^{4+} ions act as donor atoms with generating two free electrons per Mn^{4+} ion substituting one Zn^{2+} ion despite of a little amount of Mn^{4+} in the matrix of ZnO from XPS fitting result. The above supposition should be subject to further verification by the experiment. It is very intriguing that the dominant chemical state of Mn^{2+}. On one hand, the ion radii of Zn^{2+} is larger than that of Al^{3+} (0.053 nm) but nearly equal to that of Mn^{2+} (0.080 nm). In theory, the introduction of Mn^{2+} can compensate lattice distortion that derived from Al^{3+} substituting Zn^{2+}. On the other, the quantivalency of Mn^{2+} is equal to that of Zn^{2+}, i.e. it seems that Mn^{2+} ions have no donor effect and will induce to form a second new phase MnO. However, the doping level of Mn element is too small to acquire the reagent of MnO though the thermodynamics favors this kind of reaction ostensibly (cf. the forthcoming phase discussion in Section 3.3). Thus it can be deduced that the extrinsic Mn^{2+} ions will capture oxygen in competition with Zn^{2+}, which gives rise to more oxygen vacancies that can also contribute conduction electrons to be formed. In order to verify the above assumption, the O 1s core level spectra are given in Fig. 5. On the original surface of as-received film, the O 1s spectra can be resolved into three components, positioned at around 530.4 ± 0.3, 531.8 ± 0.4 and 532.4 ± 0.1 eV, respectively. The component at the low binding energy with FWHM of 2.15 eV can be ascribed to O^{2-} ions on wurtzite structure of hexagonal Zn^{2+} ion array; the intermediate one with FWHM of 2.22 eV is due to O^{2-} ions in the oxygen deficient regions; while the high binding energy peak with FWHM of 2.96 eV is corresponded to chemisorbed or dissociated –OH and OH…O type of surface species [3,17]. Hydrogen adsorbed on ZnO surface forms –OH,

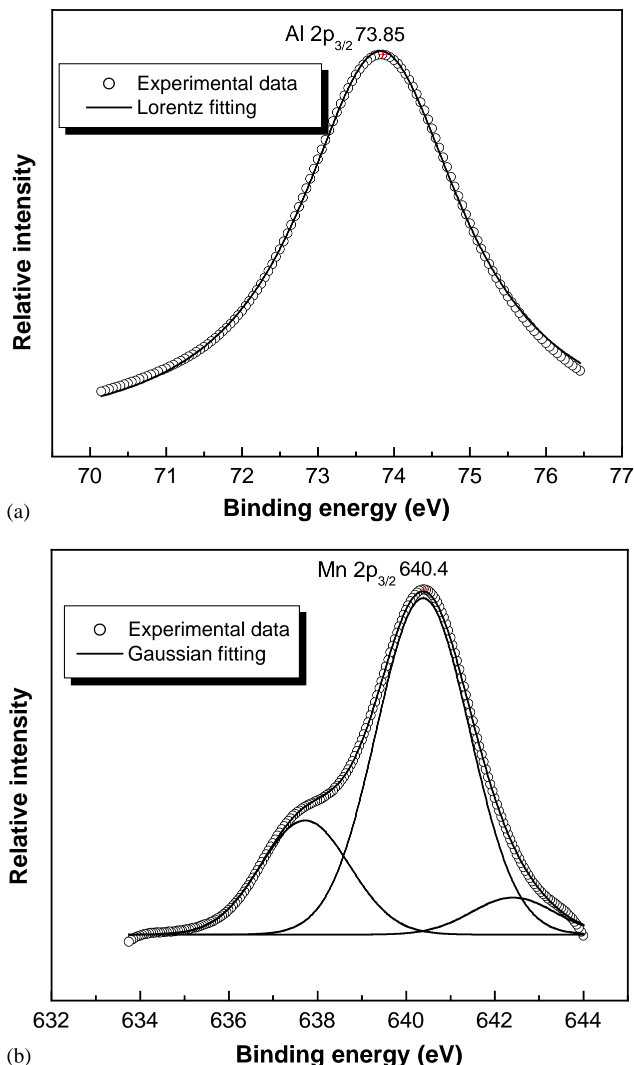

Fig. 4. XPS spectra of (a) Al $2p_{3/2}$, (b)Mn $2p_{3/2}$ after Ar^+ bombardment 4.5 nm.

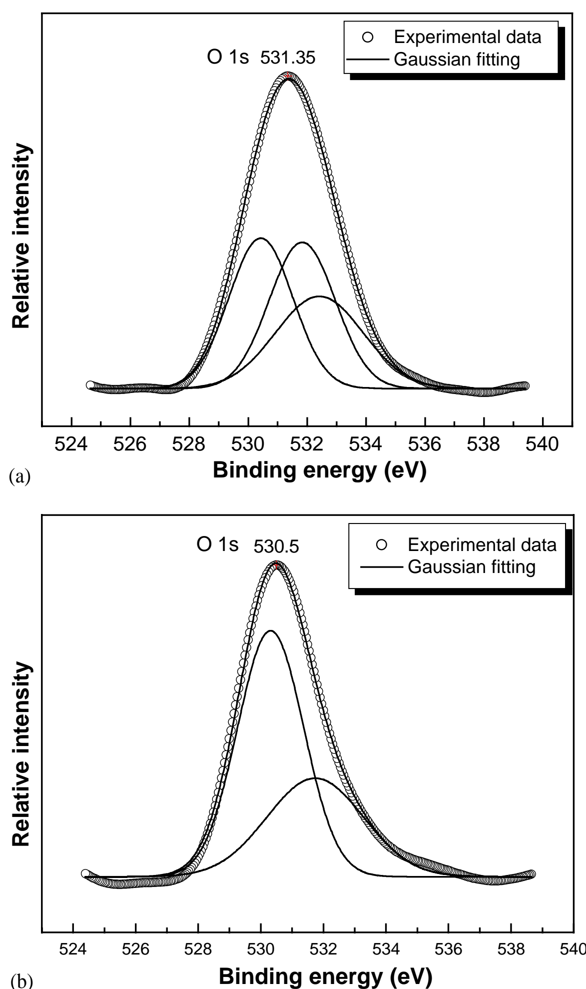

Fig. 5. O 1*s* core level region in XPS: (a) Orgianl surface, and (b) after Ar^+ etching 4.5 nm.

OH…O, Zn–H–Zn analogous loosely bonded species, which passivates the surface towards reduction by hydrogen plasma and probably accounts for why ZnO is with good chemical stability. After Ar^+ bombardment 4.5 nm, however, organic oxygen on the original surface are removed, leaving a main O 1*s* peak and a shoulder at 530.3±0.1 and 531.7±0.3 eV, respectively (cf. Fig. 5(b)). The above observation is consistent with that of Purvis et al. [18]. Moreover, the area changes of the different oxygen components are enlightening. For descriptive ease, O_{530}, O_{531}, O_{532}, O_{tot} designate the area of the component centered at 530, 531, 532 eV and the total O 1*s* peak area, respectively. On the original surface, $O_{531}/O_{tot} = 35.3\%$; while on the new surface after Ar^+ etching 4.5 nm, $O_{531}/O_{tot} = 36.9\%$, indicative of the amount of oxygen deficiency is increasing. The above contrast can be reminiscent of the aforementioned supposition, i.e. the foreign Mn^{2+} ions in the matrix of ZnO can result in more oxygen vacancies. In Fig. 6 we also display the valence band results as well as Zn 3*d* core level profiles for the pre-sputtered and post-etched

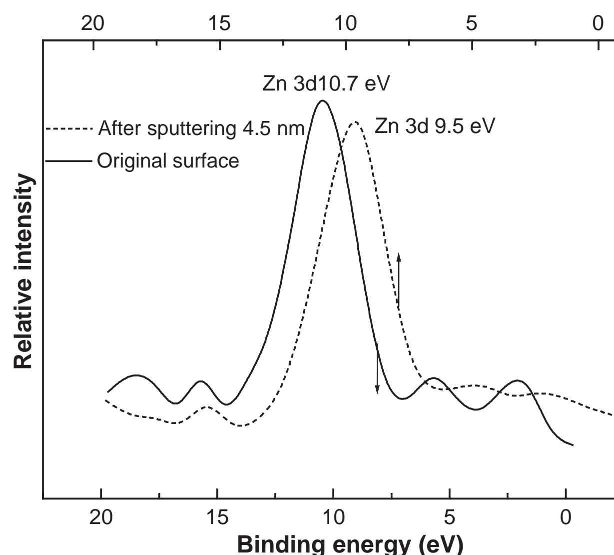

Fig. 6. Low binding energy region in XPS of ZnO: (Al, Mn) films containing valence band and Zn 3*d* core level structure before and after Ar^+ bombardment 4.5 nm.

ZnO: (Al, Mn) film surface. It is obvious that Zn 3*d* peak with spin-orbital doublet structure is shifted to a much lower binding energy (from 10.7 eV firstly to 9.5 eV latterly), relatively close to its pseudo Fermi edge (the zero reference) after Ar^+ etching. For ZnO with tetrahedral coordination structure, their point groups allow the O 2*p* and Zn 3*d* orbits to hybridize due to the small energetic separation between the $p-$ and $d-$ valence electrons [19,20], causing the valence band maximums (VBM) shift to mid gap line while the conduction band cannot be disturbed simultaneously. However, if some oxygen vacancies are present in ZnO, the Zn 3*d* and O 2*p* orbits become more localized, i.e. the effect of hybridization of $p-d$ orbitals is attenuated in conjunction with the VBM and the Zn 3*d* core level having excursion towards lower binding energy. Herein, it can be concluded that the more oxygen deficiencies are derived from the interaction between the Mn^{2+} and O^{2-} ions. In the experiment, the core level shape and position of O 1*s*, Mn $2p_{3/2}$, Al $2p_{3/2}$ and Zn $2p_{3/2}$ are nearly the same as those of post-etched 4.5 nm surface after the specimen is peeled off 16.5 nm by Ar^+ bombardment, thus the results are not given here.

3.3. Structural properties

X-ray diffraction patterns of the films deposited at various oxygen partial pressures are similar. Fig. 7(a) shows the X-ray line profile of a representative ZnO: (Al, Mn) film. Besides the (0002*n*) peaks, no Zn, Al, Mn, Al_2O_3, $ZnAl_2O_4$, MnO and MnO_2 characteristic peaks are observed, suggesting that Al and Mn co-doping does not induce distinguishable effects in X-ray spectra and other new phases (within the XRD detectable limit). It is

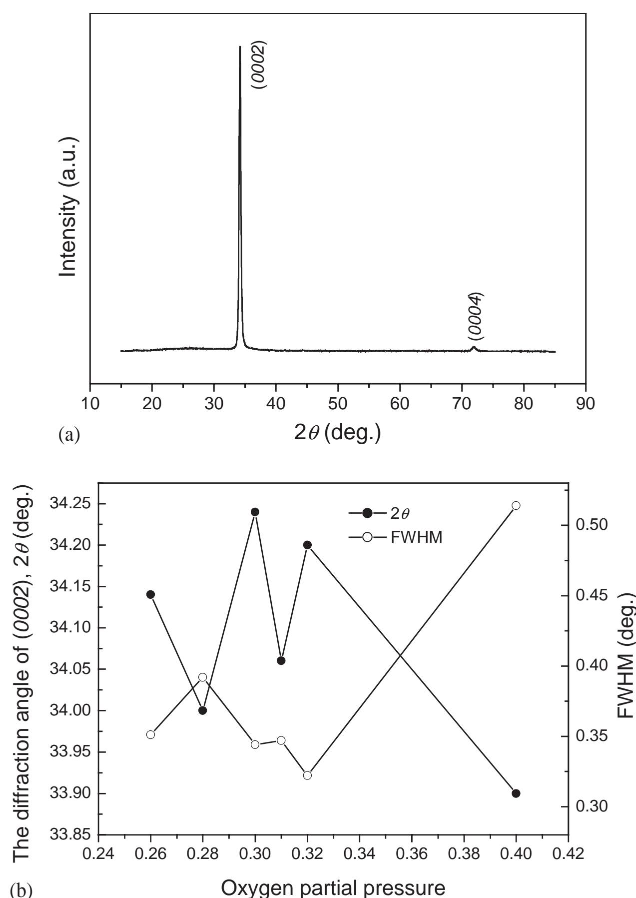

Fig. 7. (a) XRD diffraction profile of a typical ZnO: (Al, Mn) film, (b) the (0002) peak position and the full width at half-maximum of the films deposited at various oxygen partial pressure, the straight lines between measured points only serve as a guide to the eye.

considered that the structure of ZnO: (Al, Mn) films tracks that of hexagonal close-packed wurtzite-type zinc oxide and is generally polycrystalline in nature with a *c*-axis preferred orientation for all cases in this work. Information concerning position of XRD peaks and the full width at half-maximum as a function of oxygen partial pressure is displayed in Fig. 7(b). As can be seen that the (0002) peak position shifts to a lower angle with respect to the corresponding (0002) peak position of a powder standard (i.e. 34.42° in 2θ). The shift indicates that the d spacing of the (0002) planes is increasing, i.e. the unit cell is elongated along the *c*-axis. The variation of crystal constant may be the result of crystal lattice deformation related to doping or stress in the films. The average crystalline size, which is calculated from the FWHM of the (0002) peak corrected by the instrument line width broadening using Scherrer formula, is of the order of 20–30 nm.

AFM analysis reveals the films are dense and contiguous with feature of fringe crystal structure. The surface of the films is very smooth, with a root-mean-square (RMS) surface roughness $\sim 3\,\text{nm}$ over a $5 \times 5\,\mu\text{m}^2$ area by contact mode.

4. Conclusions

Transparent and conducting ZnO: (Al, Mn) films were prepared successfully by DC-reactive magnetron sputtering technique at room temperature. The effect of deposition parameters on the electro-optical, structural properties, and the surface chemical states were investigated. The lowest resistivity of $3.46 \times 10^{-4}\,\Omega\,\text{cm}$ with a Hall mobility of $32.54\,\text{cm}^2\text{V}^{-1}\text{s}^{-1}$ and a carrier density of $5.55 \times 10^{20}\,\text{cm}^{-3}$ was obtained. More than 75.0% average transmittance in the visible range from 380 to 800 nm was observed for the films coated on glass. Based on Burstein-Moss effect, the fundamental band gap, $3.48 \pm 0.01\,\text{eV}$, was calculated. The XPS analyses showed that the Zn $2p_{3/2}$ peak was almost constant with uniform chemical state of Zn^{2+} throughout the depth profile. After Ar^+ bombardment, the Al and Mn $2p_{3/2}$ ESCA peaks were detected. The Al element with uniform quantivalency of Al^{3+} acted as effective donor utility while the Mn element had more complex components. A little amount of Mn^{4+} also behaved as donor, characteristic of each Mn^{4+} substituting one Zn^{2+} ion along with releasing two free electrons into the conduction band. Mn^{2+}, the dominant component, captured oxygen in competition with Zn^{2+} in the matrix of ZnO, inducing more oxygen vacancies that contribute conduction electrons, which was confirmed from the O 1*s* XPS results. It was concluded that the presence of more oxygen deficiencies would alleviate the effect of hybridization of $p-d$ orbitals, resulting in the Zn 3*d* core level shifting to a lower binding energy. In the studied films, Zn: 4*s* donor level and oxygen vacancies could co-exist and both would contribute conduction electrons. The structure of ZnO: (Al, Mn) films tracked that of wurtizite ZnO, demonstrating a highly *c*-axis preferred orientation. Flat and smooth surface morphologies with RMS roughness $\sim 3\,\text{nm}$ over $5 \times 5\,\mu\text{m}^2$ area were observed for the as-received films.

Acknowledgments

This work was supported by National Natural Science Foundation of China (Grant No.50172051) as well as Shenyang Research Center for Interfacial Materials.

References

[1] D.C. Look, J.W. Hemsky, J.R. Sizelove, Phys. Rev. Lett. 82 (1999) 2552.

[2] R.G. Gordon, MRS Bull. 25 (2000) 52.
[3] S. Major, S. Kumar, M. Bhatnagar, K.L. Chopra, Appl. Phys. Lett. 49 (1986) 394.
[4] T. Minami, H. Sato, H. Nanto, S. Takata, Jpn. J. Appl. Phys. 24 (1985) L781.
[5] B.H. Choi, H.B. Im, J.S. Song, J. Am. Ceram. Soc. 73 (1990) 1347.
[6] D.J. Goyal, C. Agashe, M.G. Takwale, V.G. Bhide, S. Mahamuni, S.K. Kulkarni, J. Mater. Res. 8 (1993) 1052.
[7] H. Sato, T. Minami, S. Takata, J. Vac. Sci. Technol. A 11 (1993) 2975.
[8] R.P. Wang, L.L.H. King, A.W. Sleight, J. Mater. Res. 11 (1996) 1659.
[9] V. Fathollahi, M.M. Amini, Mater. Lett. 50 (2001) 235.
[10] T. Minami, T. Yamamoto, T. Miyata, Thin Solid Films 366 (2000) 63.
[11] T. Minami, MRS Bull. 25 (2000) 38.
[12] K. Ellmer, J. Phys. D: Appl. Phys. 34 (2001) 3097.
[13] H.T. Cao, Z.L. Pei, J. Gong, C. Sun, R.F. Huang, L.S. Wen, Surf. Coat. Technol., in press.
[14] E. Burstein, Phys. Rev. 93 (1954) 632.
[15] D. Auvergne, J. Camassel, H. Mathieu, Phys. Rev. B 11 (1975) 2251.
[16] R.J. Hong, X. Jiang, V. Sittinger, B. Szyszka, T. Höing, G. Bräuer, G. Heide, G.H. Frischat, J. Vac. Sci. Technol. A 20 (2002) 900.
[17] M. Chen, X. Wang, Y.H. Yu, Z.L. Pei, X.D. Bai, C. Sun, R.F. Huang, L.S. Wen, Appl. Surf. Sci. 158 (2000) 134.
[18] K.L. Purvis, G. Lu, J. Schwartz, S.L. Bernasek, J. Am. Chem. Soc. 122 (2000) 1808.
[19] S.H. Wei, A. Zunger, Phys. Rev. B 37 (1988) 8958.
[20] P. Schröer, P. Krüger, J. Pollmann, Phys. Rev. B 47 (1993) 6971.